

## Synthesis, characterization of CeO<sub>2</sub>@ZIF-8 composite abrasives and their chemical mechanical polishing behavior on glass substrate



Xiaoyue Yuan <sup>a</sup>, Chuandong Chen <sup>b</sup>, Hong Lei <sup>a,\*</sup>, Zefang Zhang <sup>c,d</sup>

<sup>a</sup> Research Center of Nano Science and Technology, College of Sciences, Shanghai University, Shanghai, 200444, China

<sup>b</sup> Baotou Rare Earth Research Institute, Inner Mongolia, 014030, People's Republic of China

<sup>c</sup> School of Chemistry and Chemical Engineering, Shanghai University of Engineering Science, Shanghai, 201620, People's Republic of China

<sup>d</sup> Shanghai Yingzhi Polishing Materials Co., Ltd., Qingpu District, Shanghai, 201700, People's Republic of China

### ARTICLE INFO

#### Keywords:

Zeolite imidazolium ester cerium oxide  
Composite abrasives  
Chemical mechanical polishing  
Polishing mechanism  
Glass substrate

### ABSTRACT

As a kind of abrasive, cerium oxide (CeO<sub>2</sub>) abrasive provides the most key support for glass planarization, whose material removal rate (MRR) is related to the concentration of Ce<sup>3+</sup> in the CeO<sub>2</sub> surface. Herein, a series of composite abrasives named zeolite imidazolium cerium oxide (CeO<sub>2</sub>@ZIF-8) were prepared to increase the concentration of Ce<sup>3+</sup> by growing different amounts of zeolitic imidazolate framework (ZIF-8) material on the cerium oxide particles, and their polishing properties on glass substrates were evaluated. When the content of ZIF-8 in the CeO<sub>2</sub>@ZIF-8 composite abrasive is 1.95 wt%, the MRR using this abrasive can reach up to 22.2 μm/h, which is 28% higher than that of pure ceria abrasive, while a lower average surface roughness (Sa, arithmetic mean height) of 1.23 nm can be obtained. The X-ray photoelectron spectroscopy results revealed an increase in the concentration of Ce<sup>3+</sup> ions in the CeO<sub>2</sub>@ZIF-8 composite abrasive surface. The contact angle tests indicated that the slurries containing CeO<sub>2</sub>@ZIF-8 abrasives had superior wettability on glass substrate. Therefore, under the synergy of the two aspects, the chemical reaction process between CeO<sub>2</sub>@ZIF-8 composite abrasives and the glass substrate is remarkably promoted, resulting in outstanding polishing performance. We believe this work adds valuable insights regarding glass CMP by using CeO<sub>2</sub>@ZIF-8 as abrasives.

### 1. Introduction

In modern manufacturing, the glass substrates' global planarity is commonly achieved by using chemical mechanical polishing (CMP) technology [1]. The rare earth oxide cerium oxide (CeO<sub>2</sub>), one of the most widely used abrasives, is considered the best abrasive for glass polishing due to its unique chemical reaction with silicon oxide (SiO<sub>2</sub>) [2]. Under the combined action of mechanical wear and chemical reaction, CeO<sub>2</sub> abrasive has a high material removal rate (MRR) and superior surface finishes. However, with the increasingly stringent requirements for planarization of glass substrates applied in advanced fields such as information display, aerospace and new energy, traditional CeO<sub>2</sub> slurry can no longer meet production needs because it is prone to agglomeration and precipitation, which is not conducive to post-wafer cleaning and may cause local roughness [3]. Therefore, the improvement of CeO<sub>2</sub> slurry and CeO<sub>2</sub> abrasive is crucial for high-precision processing across the glass industry.

The actual MRR of CeO<sub>2</sub> is closely related to its characteristics, which

will significantly affect the physicochemical properties between the CeO<sub>2</sub> abrasive and the glass surface. Zhang et al. [4] chose γ-amino-propyltriethoxysilane (APS) to directly modify CeO<sub>2</sub> nanoparticles, significantly improving the slurry's dispersion stability and reducing agglomeration. However, this modification method of cerium oxide sacrifices polishing efficiency to ensure surface quality. Cheng et al. [5] doped lanthanide elements (La, Nd, and Yb) on the CeO<sub>2</sub> surface using the modified incipient impregnation method. The MRR of doped CeO<sub>2</sub> can be increased by up to 30%, simultaneously obtaining the good surface quality (the average surface roughness is 9.3 Å). Because of the inherent valence transition characteristics of CeO<sub>2</sub>, this method can increase the concentration of Ce<sup>3+</sup> ions in the particle surface by introducing trivalent rare earth dopants to promote the conversion of Ce<sup>4+</sup> ions to Ce<sup>3+</sup> ions. This indicates that the enhanced concentration of Ce<sup>3+</sup> ions on the surface is beneficial to the decomposition of Si–O bonds and the formation of Si–O–Ce bonds during glass CMP, thereby improving the CMP performance of glass.

In addition, synthesizing composite materials is a meaningful way to

\* Corresponding author.

E-mail address: [hong\\_lei2005@aliyun.com](mailto:hong_lei2005@aliyun.com) (H. Lei).

improve the polishing performance of abrasives in recent years and has received increasing attention. The core-shell structured polystyrene@ceria/nanodiamond ternary abrasive [6] is a typical composite abrasive particle used in CMP, which reflects the synergistic effect of organic and inorganic materials, exhibiting improved CMP performance. Compared to unitary CeO<sub>2</sub> abrasive, the MRR values polished by ternary composite abrasives were 10–20% higher, and the average surface roughness values for composite abrasives were much reduced because of the combination of the nanodiamonds' high hardness, the chemical activity of CeO<sub>2</sub>, and the elastic characteristic provided by polystyrene. The composite composed of two or more components has a designable structure, which can not only maintain the advantages of the material properties of each component but also obtain comprehensive properties that a single part cannot achieve through the complementation and correlation of each component. However, like most traditional CMP, they all employ toxic and polluted ingredients during preparation, leading to potential environmental pollution [7]. To overcome these challenges, environmentally friendly compositions such as malic acid [8], chitosan oligosaccharide (COS) [9], and nicotinic acid (NA) [10] are used to develop novel green CMP slurries, making a significant contribution to the effective reduction of environmental pollution caused by conventional CMP [11]. This method offers a new idea for developing a novel CeO<sub>2</sub> CMP.

As a typical organic-inorganic hybrid zeolite imidazolate framework material, 2-Methylimidazole zinc salt (ZIF-8) is a porous crystalline material composed of zinc ions coordinated with 2-methylimidazole. It has a high specific surface area, regular pores, good thermal-chemical stability, and excellent catalytic activity [12,13]. Thus, it is widely used in the catalytic field. In addition, ZIF-8 has advantages in surface modification, allowing rational design and functionalization [14,15]. Meanwhile, ZIF-8 can be rapidly synthesized in water, avoiding the use of toxic methanol, which is beneficial for protecting the environment [16].

Inspired by these ideas, combining pure cerium oxide abrasive with ZIF-8 material may be an excellent way to promote the conversion of Ce<sup>4+</sup> ions to Ce<sup>3+</sup> ions in the cerium oxide to improve the polishing performance. Therefore, we prepared a novel CeO<sub>2</sub> composite abrasive called zeolite imidazolium ester cerium oxide (CeO<sub>2</sub>@ZIF-8) that different amounts of ZIF-8 material were grown outside the commercially available cerium oxide nucleus, and applied it in glass CMP. The microstructures and CMP behavior of CeO<sub>2</sub>@ZIF-8 composite abrasives were investigated by Fourier transform infrared spectroscopy (FTIR), scanning electron microscope (SEM), transmission electron microscope (TEM), X-ray diffraction (XRD), polishing experiments and X-ray photoelectron spectroscopy (XPS) analyses, then the polishing mechanism was further explored.

## 2. Experimental section

### 2.1. Chemicals

The chemical reagents used in all experiments are as follows. Pristine cerium oxide powders (CeO<sub>2</sub>) with an average particle size of 1 μm were purchased from Zibo Baosteel Lingzhi Rare Earth Hi-tech Co., Ltd. (China). Glutaric anhydride (C<sub>5</sub>H<sub>6</sub>O<sub>3</sub>, ≥98%), 2-methylimidazole (C<sub>4</sub>H<sub>6</sub>N<sub>2</sub>, ≥98%), and zinc nitrate hexahydrate (Zn(NO<sub>3</sub>)<sub>2</sub>•6H<sub>2</sub>O, ≥99%) were purchased from Shanghai Macklin Biochemical Co., Ltd. (China). Anhydrous ethanol (C<sub>2</sub>H<sub>5</sub>OH, ≥99.7%), N, N-dimethylformamide (DMF, C<sub>3</sub>H<sub>7</sub>NO), 3-aminopropyl triethoxysilane (KH550, C<sub>9</sub>H<sub>23</sub>NO<sub>3</sub>Si), and sodium hydroxide (NaOH), were bought from Sino-pharm Chemical Reagent Co., Ltd. (China). All chemicals were used without any further purification.

### 2.2. Synthesis of modified ceria (CeO<sub>2</sub>-COOH)

The KH550 and glutaric anhydride were used to modify the

commercially available CeO<sub>2</sub> (see Fig. 1). First, 5 g KH550 was added to a three-necked flask containing 120 mL DMF. Subsequently, 3 g glutaric anhydride was added to the mixture and stirred at room temperature for 3 h until the solution was clarified. Then, 60 mL N, N-dimethylformamide suspension (the volume ratio of DMF to H<sub>2</sub>O is 2:1) containing 40 g CeO<sub>2</sub> powder was added and stirred continuously for 5 h. After the stirring stopped, the reaction suspension was centrifuged at 5000 rpm for 5 min. Finally, the precipitate was washed twice with deionized (DI) water and anhydrous ethanol once, and dried at 60 °C for 8 h to obtain carboxylated cerium oxide powder (CeO<sub>2</sub>-COOH).

### 2.3. Preparation of CeO<sub>2</sub>@ZIF-8 composite abrasive

ZIF-8 was grown on the surface of modified CeO<sub>2</sub>-COOH by a simple method (see Fig. 1). First, 10 g of modified CeO<sub>2</sub>-COOH powder was weighed and added to a three-necked flask containing 125 g aqueous zinc nitrate hexahydrate solution, and the mixture was ultrasonicated for 10 min and stirred in a water bath at 70 °C for 30 min to evenly disperse it. Second, 375 g 2-methylimidazole aqueous solution (0.389 M) was quickly added to the suspension. After the 2-methylimidazole aqueous solution was added, the mixture was stirred for 20 min. Then, the stirring was stopped and the mixture was cooled to room temperature. Eventually, the collected reaction suspension was centrifuged at 5000 rpm for 5 min, washed twice with DI water and C<sub>2</sub>H<sub>5</sub>OH once, and dried at 80 °C for 8 h to obtain zeolite imidazolium ester cerium oxide (CeO<sub>2</sub>@ZIF-8) composite abrasives.

In order to compare the effect of ZIF-8 content on the polishing performance of CeO<sub>2</sub>@ZIF-8 composite abrasives, a series of CeO<sub>2</sub>@ZIF-8 abrasives with different ZIF-8 contents were prepared by changing the amount of Zn(NO<sub>3</sub>)<sub>2</sub>•6H<sub>2</sub>O added under the condition of a fixed concentration of 2-methylimidazole. In the end, a series of CeO<sub>2</sub>@ZIF-8 abrasives (0%, 0.50 wt%, 1.95 wt%, 3.76 wt% and 7.52 wt%, theoretically mass percentage of ZIF-8 vs. slurry) were synthesized by fixing the concentration of Zn(NO<sub>3</sub>)<sub>2</sub>•6H<sub>2</sub>O at 0, 0.019 M, 0.075 M, 0.145 M, 0.290 M, respectively.

### 2.4. Chemical mechanical polishing tests

Polishing experiments were performed by CeO<sub>2</sub> slurry, CeO<sub>2</sub>-COOH slurry, and CeO<sub>2</sub>@ZIF-8 slurries containing different ZIF-8 contents of the same solid content (2 wt%). CMP experiments were conducted by polishing glass substrates on a polishing machine (UNIPOL-1000S, Shenyang Kejing Instrument Co., LTD., China). The glass substrates used in the experiments are pristine soda lime glass substrates of constant surface roughness, and were processed into circular pieces with a diameter of 50 mm. The polishing pad is a Rodel porous polyurethane pad. The parameters of polishing were set as follows (see Table 1):

After polishing, the glass substrates were washed with detergent and DI water in sequence, dried and weighed. The MRR is calculated by

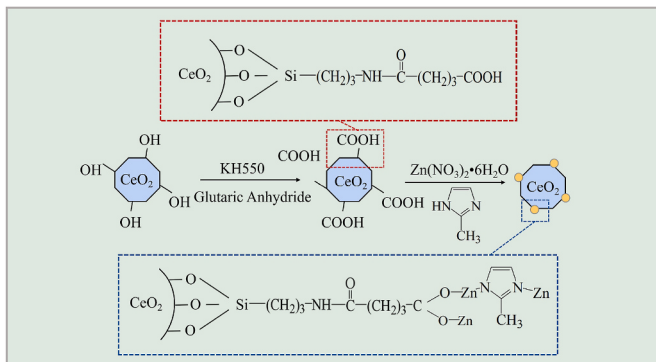


Fig. 1. Schematic diagram of the synthesis of CeO<sub>2</sub>@ZIF-8 composite abrasives.

**Table 1**

Conditions of the polishing experiment.

Parameter	Value
Amount of slurry	500 g (2 wt%)
Slurry pH	10
Polishing slurry supplying rate	180 ml/min
Wafer rotation speed	30 rpm
Pad rotation speed	60 rpm
Down force	3 kg
Polishing time	1 h

equation (1) [4,17]:

$$MRR = \frac{\Delta m * 10^4}{\rho \pi R^2 \tau} \quad (1)$$

Where, MRR: material removal rate ( $\mu\text{m}/\text{h}$ );  $\Delta m$ : mass of material removed from glass substrates before polishing and after polishing (g);  $R$ : radius of the glass substrate (cm);  $\tau$ : polishing time (h);  $\rho$ : the density of glass substrate ( $\text{g}/\text{cm}^3$ , and  $\rho_{\text{glass}} = 2.5 \text{ g}/\text{cm}^3$ ).

### 2.5. Characterization

The modification and composite process of  $\text{CeO}_2$  in the range of 4000 to  $400 \text{ cm}^{-1}$  were analyzed by FT-IR (Nicolet AVATAR 370) spectroscopy.

The morphologies of  $\text{CeO}_2$  and  $\text{CeO}_2@\text{ZIF-8}$  were characterized by SEM (JSM-7500F), and the bonding state of ZIF-8 on cerium oxide was further characterized by TEM (JSM-2010F) at 15 kV. Before the TEM test, the abrasives were diluted with ethanol, dropped onto a copper mesh, and then dried at  $80^\circ\text{C}$ .

Size distributions were obtained from a Malvern particle size analyzer (Zetasizer3000HS). Before each test, powder samples were ultrasonically dispersed in deionized water for 5 min.

XRD patterns of these samples were recorded on a D/max-2500 diffractometer (Rigaku, Japan) using  $\text{Cu K}\alpha$  radiation ( $18 \text{ kW}$ ,  $\lambda = 1.5418 \text{ \AA}$ ). The operating voltage and current of the X-ray tube were fixed at  $40 \text{ kV}$  and  $40 \text{ mA}$ , respectively. The scan speed was set at  $3^\circ \text{ min}^{-1}$  with a step size of  $0.02^\circ$ . The intensity data were collected from  $2\theta = 0$  to  $70^\circ$ .

Textural characteristics of these samples were obtained by  $\text{N}_2$ -physisorption at  $77 \text{ K}$  on an Autosorb-IQ2 physical/chemical adsorption analyzer (Quantachrome Corporation, USA). Prior to each analysis, cerium oxide and  $\text{CeO}_2@\text{ZIF-8}$  powders were rapidly heated to  $150^\circ\text{C}$  and kept at this temperature for 6 h to be degassed.

The average surface roughness ( $S_a$ , arithmetic mean height) of polished and unpolished glass substrates was measured by the S neox 090 3D surface profilometer (Sensofar, Spain) with order accuracy of 0.5%, vertical resolution of  $0.1 \text{ nm}$ , maximum lateral resolution of  $0.14 \text{ nm}$ , scanning range in the Z direction:  $0.1 \text{ nm} - 34 \text{ mm}$ , and the measurement area was  $500 \mu\text{m} \times 500 \mu\text{m}$ .

The dynamic contact angle and penetration analyzer (BIOLIN Theta Flex, Sweden) was applied to acquire the contact angle of a slurry drop on the surface of a glass substrate. Before the measurement, the polished substrates were cleaned with deionized water and then dried. Measurements were repeated 5 times for each substrate, and take the average value to ensure the accuracy of the experimental data.

The element compositions of  $\text{CeO}_2$  and  $\text{CeO}_2@\text{ZIF-8}$  abrasives were studied by XPS (ESCALAB 250Xi). The XPS spectrum was obtained by focusing monochromatized  $\text{Al K}\alpha$  radiation and calibrated by applying an exogenous C 1s signal at 284.6 eV.

## 3. Results and discussions

### 3.1. Structure and morphology analysis of $\text{CeO}_2@\text{ZIF-8}$ composite abrasives

#### 3.1.1. FT-IR analysis

FT-IR spectra (Fig. 2) were used to characterize the functional groups present on the surface of  $\text{CeO}_2$ , carboxylated  $\text{CeO}_2-\text{COOH}$ , and synthesized  $\text{CeO}_2@\text{ZIF-8}$  (0.50 wt%). The typical absorption peak of  $\text{CeO}_2$  is the Ce–O stretching band at  $470 \text{ cm}^{-1}$  [18,19], which was also found in the as-prepared particles. The broadband around  $3400 \text{ cm}^{-1}$  corresponds to the hydrated hydroxyl group of cerium oxide before modification. This band is slightly shifted to  $3424 \text{ cm}^{-1}$  after carboxylated modification, which may be explained by the absorption superposition of  $-\text{OH}$  and  $-\text{NH}_2$  groups [4]. It is worth noting that the prominent peaks of  $\text{CeO}_2-\text{COOH}$  were found at  $1651 \text{ cm}^{-1}$  ( $\text{C=O}$  stretching vibration) and  $1454 \text{ cm}^{-1}$  ( $\text{C-N}$  stretching vibration), respectively [20]. The  $-\text{OH}$  broadband on the  $\text{CeO}_2@\text{ZIF-8}$  (0.50 wt%) curve disappears at  $3424 \text{ cm}^{-1}$  and  $1651 \text{ cm}^{-1}$ , which proves the combination of carboxylic acid and ZIF-8. At the same time, the dense peaks at  $700-1500 \text{ cm}^{-1}$  are due to the stretching and plane vibration of ZIF-8 [15]. Thus,  $\text{CeO}_2-\text{COOH}$  was prepared, and the zeolite imidazolate material ZIF-8 was successfully grown on the surface of  $\text{CeO}_2-\text{COOH}$ .

#### 3.1.2. XRD analysis

The XRD patterns (Fig. 3) were further used to confirm the successful formation of ZIF-8 on  $\text{CeO}_2@\text{ZIF-8}$  (0.50 wt%). The diffraction peaks at  $28.5^\circ$ ,  $33.1^\circ$ ,  $47.5^\circ$ ,  $56.3^\circ$ ,  $59.1^\circ$ , and  $69.4^\circ(20)$  were sharp and intense, indicating their highly crystalline nature, which is consistent with the diffraction of standard cubic fluorite-phase  $\text{CeO}_2$  (PDF#81-0792). Furthermore, the remaining peaks are ascribed to the reflection of the ZIF-8 grown outside cerium oxide [16]. The reason for these ZIF-8 peaks with low intensity is due to their lower loading content (the mass ratio of ZIF-8 to  $\text{CeO}_2@\text{ZIF-8}$  is 1: 5) and weak crystallization. The XRD pattern confirmed the coexistence of ceria dioxide and ZIF-8 in  $\text{CeO}_2@\text{ZIF-8}$  composite abrasives.

#### 3.1.3. SEM images and size distribution

SEM micrographs (Fig. 4a-d) show the typical morphologies of  $\text{CeO}_2$  and  $\text{CeO}_2@\text{ZIF-8}$  (0.50 wt%) abrasives under low and high magnification. Fig. 4c shows that pure  $\text{CeO}_2$  abrasive has an angulated shape and

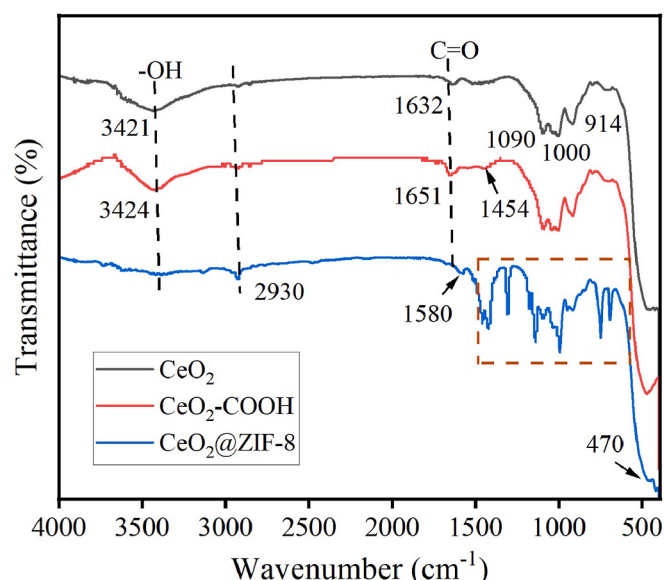
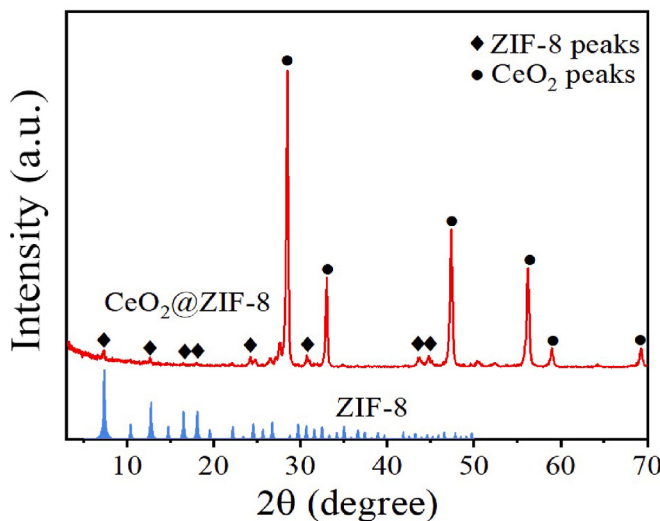


Fig. 2. FT-IR spectra of  $\text{CeO}_2$ ,  $\text{CeO}_2-\text{COOH}$  and  $\text{CeO}_2@\text{ZIF-8}$  (0.50 wt %) particles.



**Fig. 3.** XRD pattern of prepared CeO<sub>2</sub>@ZIF-8 (compared with ZIF-8 standard PDF cards).

severe aggregation. The edge of the synthesized CeO<sub>2</sub>@ZIF-8 (0.50 wt%) is not as sharp as that of pure CeO<sub>2</sub> owing to the presence of uneven and soft ZIF-8 material on the surface (Fig. 4d). Referring to the inserted particle size distribution images, it can be intuitively observed that the size distribution curve of CeO<sub>2</sub>@ZIF-8 (0.50 wt%) composite abrasive is more concentrated and the average particle size is slightly smaller than that of pure CeO<sub>2</sub>, which indicates that the agglomeration of composite abrasives was alleviated.

Fig. 4e shows the size distribution of CeO<sub>2</sub> particles and different CeO<sub>2</sub>@ZIF-8 particles. Compared to pure CeO<sub>2</sub> abrasive, all the CeO<sub>2</sub>@ZIF-8 abrasives show a narrow particle distribution, and the sizes of the composite particles all decrease. This may be explained by the presence of ZIF-8. The organic imidazolyl groups and metallic Zn<sup>2+</sup> ions of ZIF-8 provide a stronger steric effect for the composite particles, thus

effectively preventing agglomeration between CeO<sub>2</sub> particles. It's well known that improving dispersion stability helps to reduce mechanical damage, which is usually caused by hard agglomeration in polishing slurries [4]. The average diameters of CeO<sub>2</sub>@ZIF-8 abrasives are not only smaller than those of pure CeO<sub>2</sub> particles, but also more uniform and concentrated. Therefore, the dispersibility of the CeO<sub>2</sub> composite particles is indeed improved.

### 3.1.4. TEM images

The detailed structure can be further investigated by TEM. By comparing Fig. 5a and Fig. 5c, we can intuitively see that both the light and dark regions exist in the image of CeO<sub>2</sub>@ZIF-8 (0.50 wt%) composite abrasive (Fig. 5c), while pure cerium oxide has no light area. The dark region of the individual particle is CeO<sub>2</sub> and the light area is ZIF-8. In other words, the ZIF-8 materials are anchored over the CeO<sub>2</sub> hosts since the bright and dark areas are closely combined. The results of energy dispersion spectroscopy (EDS) of area A in CeO<sub>2</sub> and area B in CeO<sub>2</sub>@ZIF-8 composite particle (two regions in the transmission electron microscope image) are shown in Fig. 5b and Fig. 5d, respectively. The result of CeO<sub>2</sub>@ZIF-8 (0.50 wt%) shows that elements of Ce, O, Zn, and Si exist simultaneously on the outer surface of cerium oxide grown by ZIF-8 (area B, see Fig. 5d). In contrast, there is no Zn peak and Si peak in the EDS results of pure cerium oxide. This means that ZIF-8 is immobilized on cerium oxide under the action of a silane coupling agent. Thus, we can conclude that the nucleation and growth of ZIF-8 on CeO<sub>2</sub>@ZIF-8 abrasive particles were strictly confined to the outer surface of cerium oxide. In addition, a high percentage of Cu elements comes from the copper mesh of TEM test.

### 3.1.5. BET test

Brunauer–Emmett–Teller (BET) gas adsorptiometry measurements were performed to obtain the pore properties of CeO<sub>2</sub> and CeO<sub>2</sub>@ZIF-8. Fig. 6 shows the N<sub>2</sub> adsorption/desorption isotherm (a) and the pore-size distribution of CeO<sub>2</sub> and CeO<sub>2</sub>@ZIF-8 abrasives (b). The isotherms are identified as the classical IV-type isotherm with an obvious type H3 hysteresis loop as defined by IUPAC, which indicates that a mesopore (the pore diameter ( $d$ ) is 2–50 nm) structure exists in these samples [21].

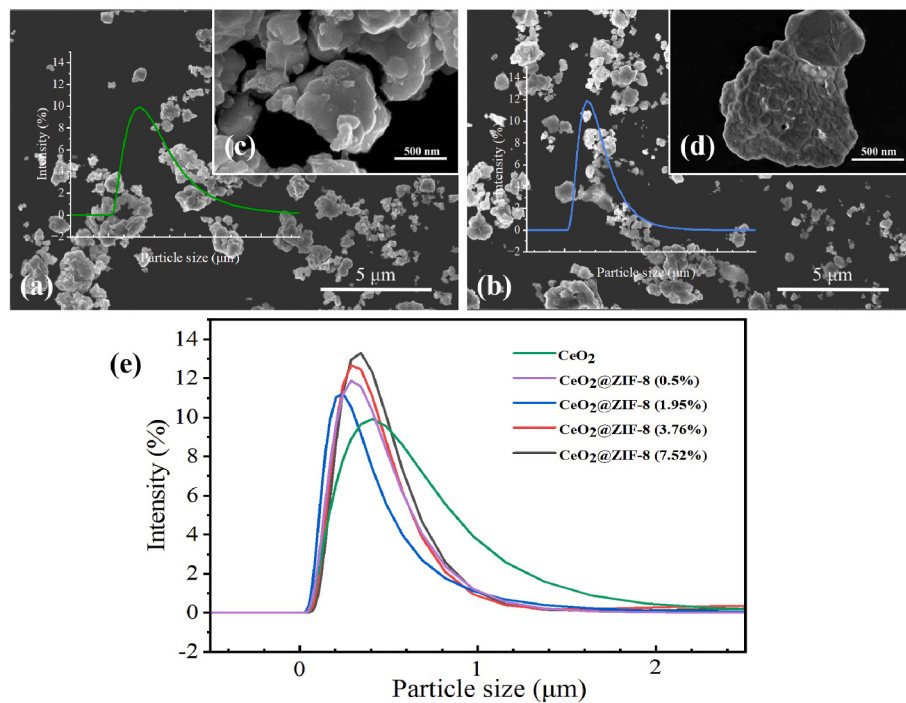


**Fig. 4.** SEM images of (a, c) CeO<sub>2</sub> and (b, d) CeO<sub>2</sub>@ZIF-8 (0.50 wt%) particles; (e) Size distribution of CeO<sub>2</sub> and CeO<sub>2</sub>@ZIF-8 abrasives (pH = 10). The insets in (a, b) are the respective particle size distributions.

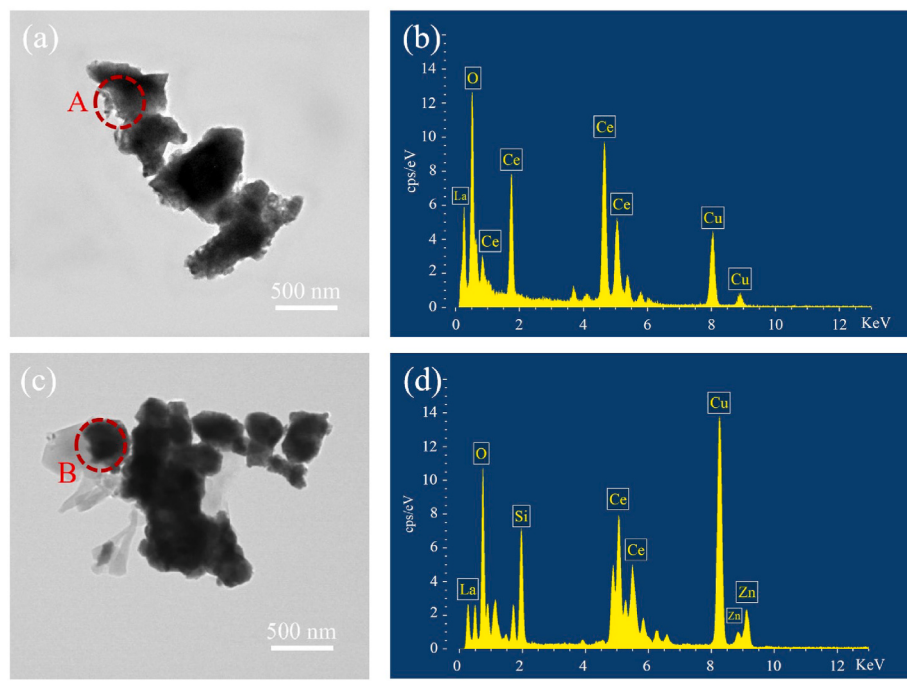


**Fig. 5.** TEM images of (a) pure CeO<sub>2</sub> and (c) CeO<sub>2</sub>@ZIF-8 (0.50 wt%) abrasives; (b, d) EDS element analysis images of A and B, respectively.

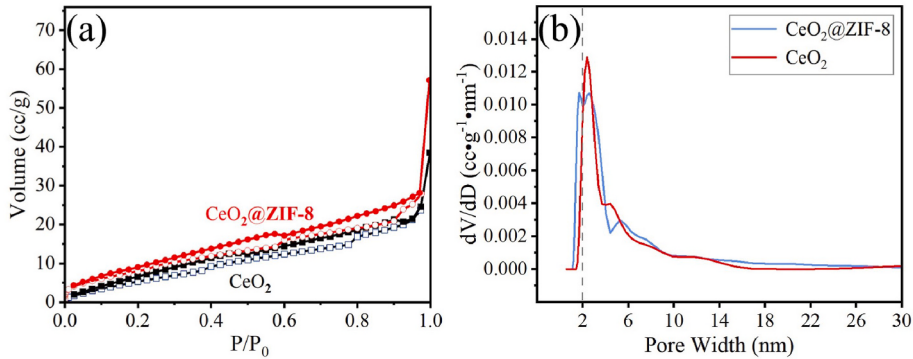


**Fig. 6.** N<sub>2</sub> adsorption-desorption isotherms (a) and pore size distribution curves (b) of CeO<sub>2</sub> and CeO<sub>2</sub>@ZIF-8 (0.50 wt%) abrasives (Empty symbols: adsorption, filled symbols: desorption; The grey dotted line is the boundary between the microporous and mesoporous regions).

The values of the BET surface area ( $S_{\text{BET}}$ ), total pore volume ( $V_{\text{DFT}}$ ), and pore diameter are listed in Table 2, choosing the multi-point Brunauer-Emmett-Teller (BET) method for calculating the specific surface area and using the density functional theory (DFT) method for obtaining the pore distribution. We find that the BET-specific surface area increases with the loading of ZIF-8 on the surface of CeO<sub>2</sub>. Furthermore, the total pore volume of CeO<sub>2</sub>@ZIF-8 increases obviously after the introduction of ZIF-8, suggesting that microporous ZIF-8 is mainly located on the outer surface of CeO<sub>2</sub>. Finally, the pore width ( $d$ ) of CeO<sub>2</sub>@ZIF-8 located in the mesopore range is 1.682 nm, which is smaller than that of CeO<sub>2</sub>. We can see from Fig. 6b that the pore size distribution of CeO<sub>2</sub> reveals its micropore structure, while CeO<sub>2</sub>@ZIF-8 has a peak in the microporous area ( $d < 2$  nm) due to the growth of microporous ZIF-8.

**Table 2**  
Textural properties of CeO<sub>2</sub> and CeO<sub>2</sub>@ZIF-8 (0.50 wt%).

Sample	$S_{\text{BET}}$ [m <sup>2</sup> /g]	$V_{\text{DFT}}$ [cc/g]	Pore diameter (nm)
CeO <sub>2</sub>	27.172	0.034	2.382
CeO <sub>2</sub> @ZIF-8	36.569	0.041	1.682

The above facts illustrate that the prepared CeO<sub>2</sub>@ZIF-8 composite abrasive has a larger specific surface area and pore volume than the original cerium oxide, which is conducive to enhancing the hydrophilicity of the abrasives, thereby increasing the contact area between the glass surface and the slurry.

### 3.2. CMP performance

MRR is a critical indicator for evaluating polishing performance. Fig. 7 shows the MRRs of the slurries prepared by CeO<sub>2</sub>, CeO<sub>2</sub>-COOH, and CeO<sub>2</sub>@ZIF-8 (0.50 wt%). Under the same polishing conditions, the MRR of CeO<sub>2</sub>@ZIF-8 (0.50 wt%) was 19.24 μm/h, which is increased by 11% compared with that of the pure ceria slurry (17.34 μm/h) and also higher than that of CeO<sub>2</sub>-COOH. This indicates that the CeO<sub>2</sub>@ZIF-8 composite abrasive has a significantly improved polishing rate for glass.

To further determine the optimum ZIF-8 content in CeO<sub>2</sub>@ZIF-8 particles, different contents were analyzed. Fig. 8 shows the effect of CeO<sub>2</sub> abrasives and CeO<sub>2</sub>@ZIF-8 composite abrasives with different ZIF-8 contents on the MRR. It can be seen from the trend of broken lines that the MRR increases with increasing ZIF-8 content at the beginning, which may be because the chemical activity of abrasives increases with the rise

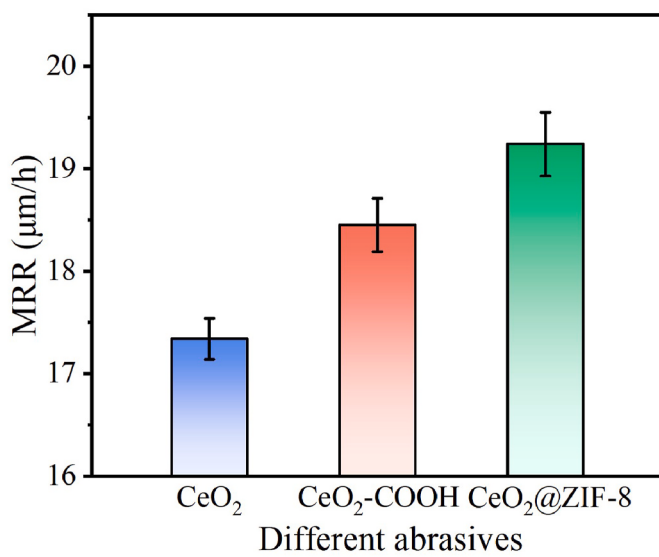


Fig. 7. The MRRs of  $\text{CeO}_2$ ,  $\text{CeO}_2\text{-COOH}$  and  $\text{CeO}_2@\text{ZIF-8}$  (0.50 wt%) abrasives.

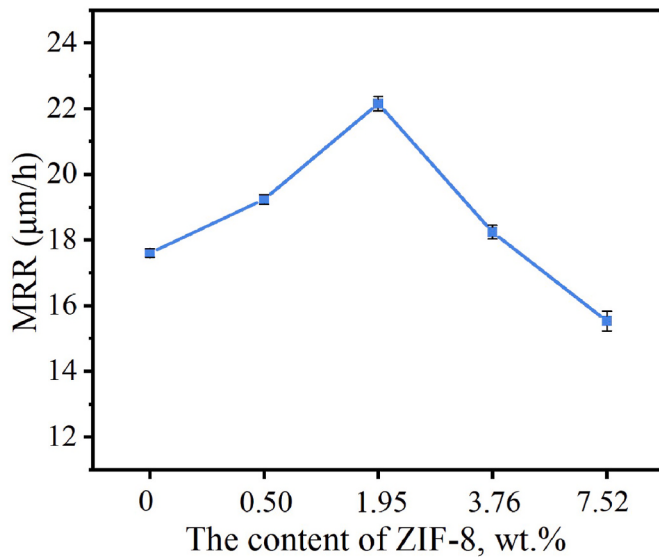


Fig. 8. The effect of the content of ZIF-8 on MRR.

of ZIF-8 content, thus improving the polishing rate. When the content of ZIF-8 is 1.95 wt%, the synergistic effect of chemical and mechanical impact may be optimally balanced, and the MRR reaches the maximum value (22.15  $\mu\text{m}/\text{h}$ ). In addition, referring to the size distribution (Fig. 4e), the improved dispersibility of the composite abrasives is also conducive to enhancing the MRR. When the content of ZIF-8 continues to increase, the MRR begins to decline because a large amount of ZIF-8 decreases the overall mechanical hardness of the composite abrasive.

Fig. 9 shows the three-dimensional surface profile of the glass substrates before and after polishing by pure  $\text{CeO}_2$  and  $\text{CeO}_2@\text{ZIF-8}$  composite abrasives with different ZIF-8 contents. Compared with the glass substrate with significant roughness before polishing ( $\text{Sa} = 1.96 \text{ nm}$ ), the surfaces of glass substrates (Fig. 9b–e) polished by  $\text{CeO}_2@\text{ZIF-8}$  composite abrasives are smoother and without obvious bulges. Furthermore, Fig. 10 intuitively presents the change in  $\text{Sa}$  of glass substrates polished by pure  $\text{CeO}_2$  and different  $\text{CeO}_2@\text{ZIF-8}$  composite abrasives. When using  $\text{CeO}_2@\text{ZIF-8}$  (1.95 wt%) abrasives, the highest MRR and the lowest  $\text{Sa}$  ( $\text{Sa} = 1.23 \text{ nm}$ ) can be simultaneously obtained, which means that  $\text{CeO}_2@\text{ZIF-8}$  (1.95 wt%) composite abrasives can

effectively improve the surface quality of polished glass. The reason is that ZIF-8, a zeolite-like metal-organic framework material, is softer than  $\text{CeO}_2$ , which can mitigate the hard damage to glass caused by cerium oxide agglomeration [4,22]. However, when the content of ZIF-8 is more significant than 1.95 wt%, excessive ZIF-8 will reduce the hardness and mechanical properties of  $\text{CeO}_2@\text{ZIF-8}$  composite abrasives, further preventing the effective grinding of rough peaks on the glass surface. As a result, the  $\text{Sa}$  values of composite abrasives in Fig. 9e and f increase.

In summary, the polishing performance on glass substrates using  $\text{CeO}_2@\text{ZIF-8}$  composite abrasives is improved; the best content of ZIF-8 of  $\text{CeO}_2@\text{ZIF-8}$  abrasive is 1.95 wt%, which can achieve superior polishing performance with a minimum  $\text{Sa}$  of 1.23 nm.

### 3.3. Analysis of the polishing mechanism

CMP is a combination of mechanical grinding and chemical etching, and the best CMP performance can be achieved only when the two effects are well balanced. Numerous attempts have been made to explain the chemical and mechanical effects behind cerium oxide polishing [23–25]. Considering the effects of these two aspects, the CMP mechanism of  $\text{CeO}_2@\text{ZIF-8}$  abrasives on glass substrates was studied by using contact angle and XPS tests. What's more, we propose a schematic diagram of the possible mechanism of  $\text{CeO}_2@\text{ZIF-8}$  composite abrasives in the polishing process.

We carried on a contact angle measurement to characterize the interaction between  $\text{CeO}_2@\text{ZIF-8}$  particles and glass substrates. Fig. 11 shows the contact angle of the  $\text{CeO}_2@\text{ZIF-8}$  slurries with different ZIF-8 contents. It can be observed that the contact angle of  $\text{CeO}_2$  slurry on the glass is  $65.8^\circ$ , and then the contact angle of  $\text{CeO}_2@\text{ZIF-8}$  abrasives decreases as the loading of ZIF-8 increases. This result indicates that the wettability of  $\text{CeO}_2@\text{ZIF-8}$  slurries on the glass substrates is enhanced, which is due to the elastic deformation of the  $\text{CeO}_2@\text{ZIF-8}$  abrasives and the presence of imidazole rings in ZIF-8. In addition, the surface of cerium oxide in alkaline solution is negatively charged, as is the surface of the glass, while ZIF-8 is positively charged due to the presence of the central  $\text{Zn}^{2+}$  ion, so the electrostatic repulsion force of  $\text{CeO}_2@\text{ZIF-8}$  slurries is smaller than that of pure cerium oxide slurry, which also contributes to the reduction of the contact angle [26]. A smaller contact angle accounts for better interfacial wettability, which enhances the chemical reaction at the solid-liquid interface [27]. Thus, it can increase the contact area during the CMP process, which benefits the chemical and mechanical action. Ding et al. [28] found that the MRR is positively correlated with the contact area of abrasives and the number of effective particles. It means a larger contact area with the glass and easier attachment of particles to the glass substrate surface. Thus, compared to pure  $\text{CeO}_2$  particles, the MRRs of  $\text{CeO}_2@\text{ZIF-8}$  composite abrasives are improved.

Although cerium in  $\text{CeO}_2$  exists in the form of  $\text{Ce}^{4+}$  ions, due to oxygen deficiency,  $\text{Ce}^{3+}$  and  $\text{Ce}^{4+}$  ions coexist in the surface of  $\text{CeO}_2$ . To analyze the differences in the element oxidation states of  $\text{CeO}_2$  and  $\text{CeO}_2@\text{ZIF-8}$  composite abrasives, XPS was further used. Fig. 12a shows the photoelectron spectra of ceria particles before and after compositing. Both the pure ceria particles (curve a) and composite ceria particles (curve b–e) give peaks of elements of Ce, C, and O, while new peaks of Zn and N elements appear in the  $\text{CeO}_2@\text{ZIF-8}$  composite abrasives.

Semi-quantitative calculation of  $\text{Ce}^{3+}$  content in the  $\text{CeO}_2@\text{ZIF-8}$  nanoparticles can be conducted by peak deconvolution of XPS spectra to track how the ZIF-8 material affects the polishing performance of  $\text{CeO}_2@\text{ZIF-8}$ . In the case of ceria, orbital splitting and a series of energy transfer processes between electrons create a total of ten photoelectron peaks in the Ce 3d spectrum [29]. These ten deconvolution peaks (see Fig. 12b) are labeled u,  $u_0$ ,  $u'$ ,  $u''$ ,  $u'''$ , v,  $v_0$ ,  $v'$ ,  $v''$ , and  $v'''$ , as shown in Table 3 [30]. Among them, six peaks ( $u$ ,  $u''$ ,  $u'''$ , v,  $v''$ ,  $v'''$ ) correspond to  $\text{Ce}^{4+}$  while the other four ( $v_0$ ,  $v'$ ,  $u_0$ ,  $u'$ ) are associated with  $\text{Ce}^{3+}$ . By measuring the area of each peak, the concentration of  $\text{Ce}^{3+}$  on the

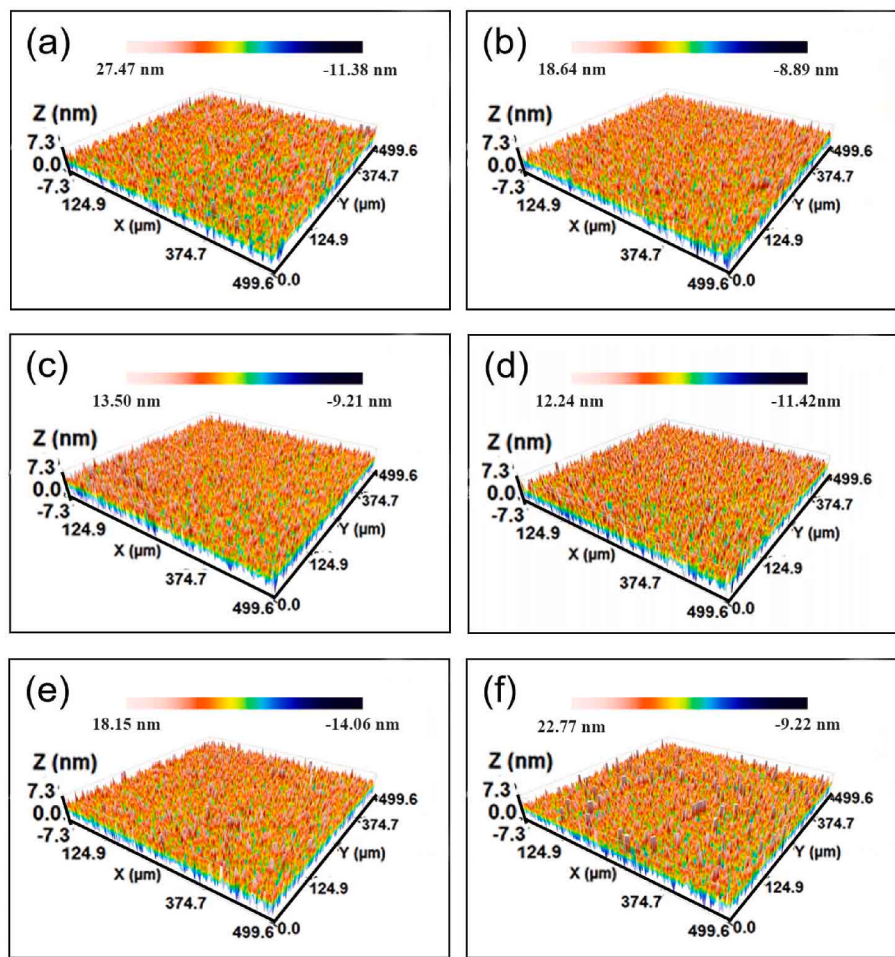


**Fig. 9.** Surface profiles of glass substrates: (a) unpolished,  $S_a = 1.96 \text{ nm}$ ; (b) polished by  $\text{CeO}_2$ :  $S_a = 1.55 \text{ nm}$ ; (c) polished by  $\text{CeO}_2@\text{ZIF-8}$  (0.50 wt%):  $S_a = 1.50 \text{ nm}$ ; (d) polished by  $\text{CeO}_2@\text{ZIF-8}$  (1.95 wt%):  $S_a = 1.23 \text{ nm}$ ; (e) polished by  $\text{CeO}_2@\text{ZIF-8}$  (3.76 wt%):  $S_a = 1.44 \text{ nm}$ ; (f) polished by  $\text{CeO}_2@\text{ZIF-8}$  (7.52 wt%):  $S_a = 1.63 \text{ nm}$ .

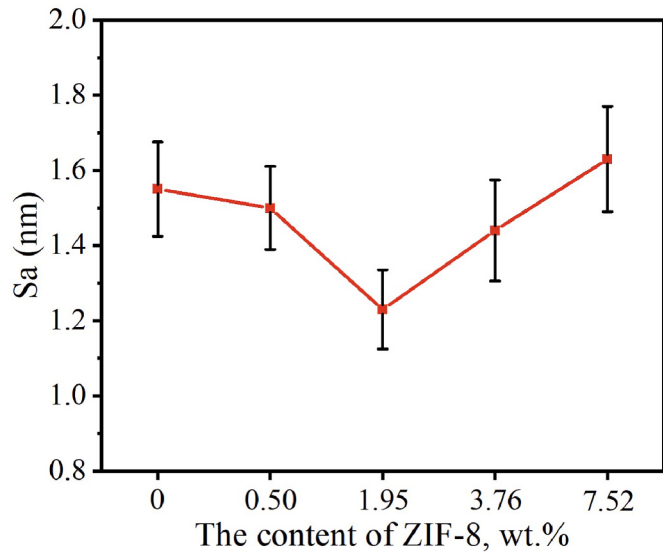


**Fig. 10.** The effect of the content of ZIF-8 on  $S_a$  ( $S_a$  before polishing was 1.96 nm).

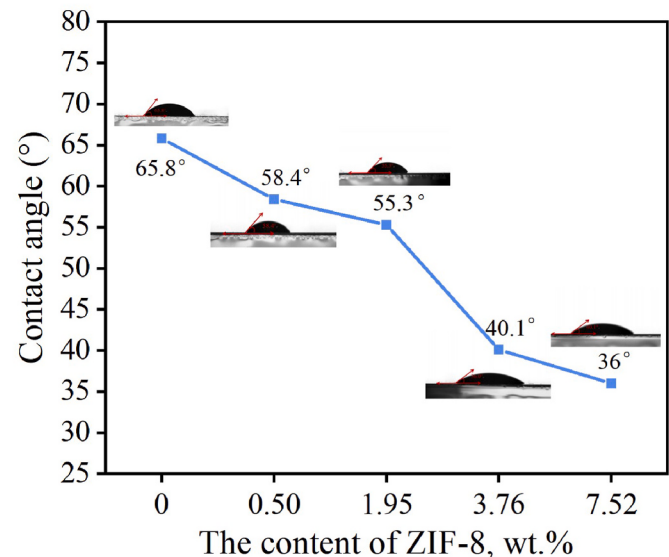


**Fig. 11.** The contact angle of slurries with different ZIF-8 contents.

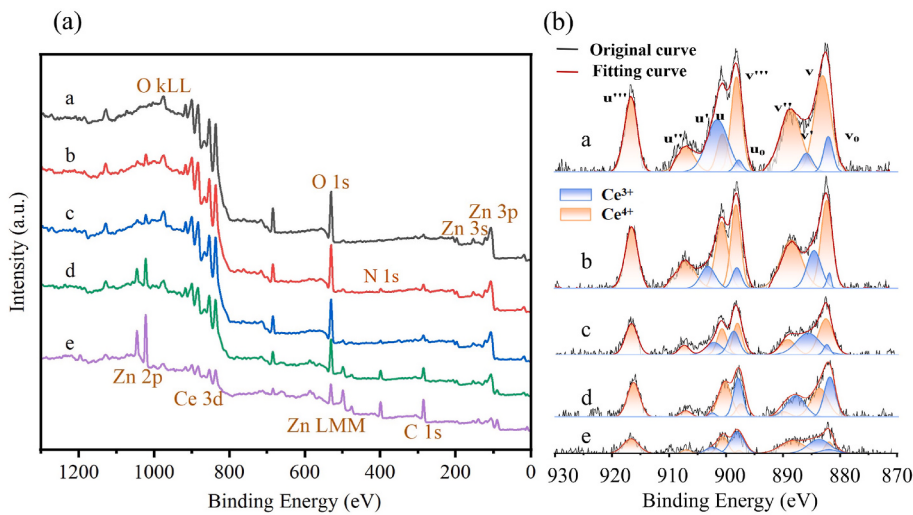


**Fig. 12.** (a) The photoelectron spectra of CeO<sub>2</sub> before and after compositing; (b) XPS narrow scan spectra of Ce 3d element and the peak deconvolution of CeO<sub>2</sub> and CeO<sub>2</sub>@ZIF-8 (curve a: CeO<sub>2</sub>; curve b–e: CeO<sub>2</sub>@ZIF-8: 0.50 wt%, 1.95 wt%, 3.76 wt%, 7.52 wt%, respectively).

**Table 3**

Peak deconvolution parameters for the Ce 3d XPS spectrum in Fig. 12 (b).

	Ce <sup>3+</sup>				Ce <sup>4+</sup>					
	v <sub>0</sub>	v'	u <sub>0</sub>	u'	v	v''	v'''	u	u''	u'''
Binding energy (eV)	880.6	885.4	898.9	904	882.6	888.8	898.4	901	907	916.7

surfaces of the abrasives can be calculated through the following equation (2) [31]:

$$C(Ce^{3+}) = \frac{A(u_0) + A(u') + A(v_0) + A(v')}{A(u_0) + A(u) + A(u') + A(u'') + A(u''') + A(v_0) + A(v) + A(v') + A(v'') + A(v''')} \times 100 \quad (2)$$

Where, C represents the concentration of Ce<sup>3+</sup> and A is the area of each fitting peak. As a result, the calculated concentration of CeO<sub>2</sub> and a series of CeO<sub>2</sub>@ZIF-8 based on the fraction of area (Ce<sup>3+</sup>) in the total area (Ce<sup>3+</sup> and Ce<sup>4+</sup>) are shown in Table 4. The concentration of Ce<sup>3+</sup> in pristine CeO<sub>2</sub> is only 26.4%. The concentration of Ce<sup>3+</sup> significantly increases with a higher content of ZIF-8 material grown on the surface of CeO<sub>2</sub> abrasives, from 26.4% to 28.6%, 37.5%, 42.0%, and 46.3%, respectively. This result demonstrates that the concentration of Ce<sup>3+</sup> ions in the surface of the CeO<sub>2</sub>@ZIF-8 composite abrasives is enhanced.

According to the mechanism proposed by Kelsall et al. [32,33], the presence of active sites Ce<sup>3+</sup> in the surface of ceria abrasives can promote the chemical interaction between ceria abrasives and glass. Therefore, the increased concentration of Ce<sup>3+</sup> ions in the CeO<sub>2</sub>@ZIF-8 composite abrasives is another critical reason for the increase of the MRR [34]. Since the Zn<sup>2+</sup> cations are smaller in size than Ce<sup>4+</sup> cations, the combination of ZIF-8 on the CeO<sub>2</sub> surface leads to the formation of more oxygen vacancies in the cerium lattice, as shown in Fig. 13a. The

obtained oxygen deficiency promotes oxygen diffusion so that oxygen would move to inner ceria particles according to thermodynamic sta-

bility, and thus more Ce<sup>3+</sup> ions would be exposed to the surface of CeO<sub>2</sub>@ZIF-8 abrasives [35]. With the help of some ions in the aqueous solution, these Ce<sup>3+</sup> ions can provide electrons to the antibonding orbital of the Si–O bond, weakening and stretching the Si–O bond. They not only promote the formation of the glass hydration layer, but also facilitate the generation of the Ce–O–Si bonds that are stronger than Si–O–Si [36], effectively improving the polishing performance of CeO<sub>2</sub>@ZIF-8 abrasives on glass substrate. The possible polishing mechanism involved in the glass CMP process is shown in Fig. 13b.

Based on the above analysis, on the one hand, CeO<sub>2</sub>@ZIF-8 composite abrasives combined with ZIF-8 are more easily absorbed by the glass surface due to the reduction of contact angle during polishing, which increases the contact area with the glass substrate and makes the number of effective particles increase obviously. On the other hand, an increase in the concentration of active site Ce<sup>3+</sup> in the CeO<sub>2</sub>@ZIF-8 particle surface enhances the chemical effect in CMP. Therefore, compared with pure CeO<sub>2</sub> abrasive, the CeO<sub>2</sub>@ZIF-8 composite abrasives have stronger chemical reaction activity with glass, bringing

**Table 4**

The calculated concentration of CeO<sub>2</sub> and a series of CeO<sub>2</sub>@ZIF-8 from XPS spectra.

	CeO <sub>2</sub>	CeO <sub>2</sub> @ZIF-8 (0.50 wt%)	CeO <sub>2</sub> @ZIF-8 (1.95 wt%)	CeO <sub>2</sub> @ZIF-8 (3.76 wt%)	CeO <sub>2</sub> @ZIF-8 (7.52 wt%)
Concentration of Ce <sup>3+</sup> (%)	26.4	28.6	37.5	42.0	46.3

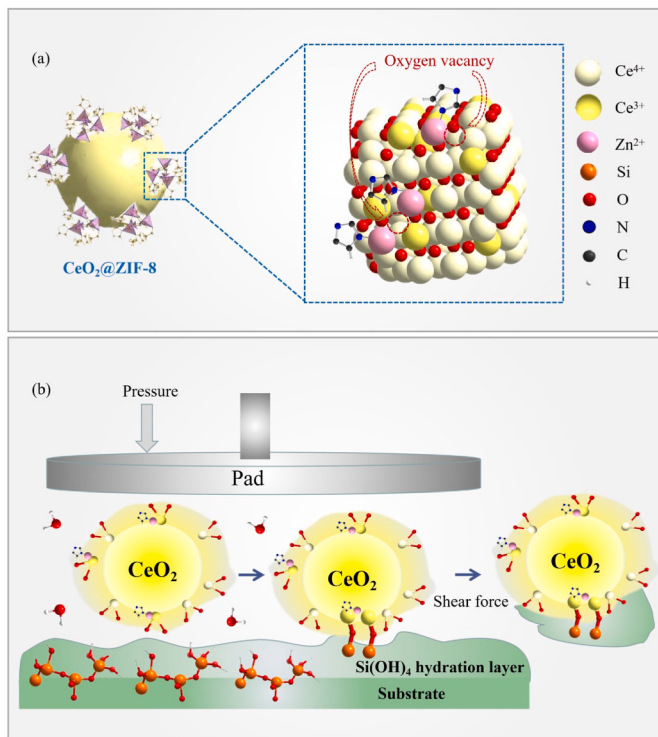


**Fig. 13.** (a) The space filling model of the CeO<sub>2</sub>@ZIF-8 surface structure; (b) the mechanism for polishing glass with CeO<sub>2</sub>@ZIF-8 composite abrasives.

superior polishing performance. However, the organic ZIF-8 material itself is softer than the glass substrate. Excessive ZIF-8 on CeO<sub>2</sub> particles will enhance the lubrication between the particles and the surface of the glass substrate, and significantly reduce the mechanical effect of the abrasive. Thus, the proper amount of ZIF-8 in CeO<sub>2</sub>@ZIF-8 composite abrasives is vital to obtain the high CMP rate.

#### 4. Conclusions

CeO<sub>2</sub>@ZIF-8 abrasives were synthesized by growing ZIF-8 on the surface of CeO<sub>2</sub> particles through the in-situ method. The CeO<sub>2</sub>@ZIF-8 abrasives exhibited a higher MRR and much better surface quality than the pure CeO<sub>2</sub> abrasive under the same polishing conditions. Especially when the content of ZIF-8 is 1.95 wt%, the CeO<sub>2</sub>@ZIF-8 abrasive can reach the maximum MRR value (22.2 μm/h) and simultaneously obtain the lowest surface roughness (Sa = 1.23 nm). The polishing mechanism is further explored by XPS analysis and contact angle measurements. The increasing contact area with the glass substrate and an increase in the concentration of active site Ce<sup>3+</sup> on the CeO<sub>2</sub>@ZIF-8 surface synergistically contribute to the stronger chemical reaction activity between CeO<sub>2</sub>@ZIF-8 composite abrasives and glass substrate, thus bringing superior CMP performance.

#### Declaration of competing interest

The authors declare that they have no known competing financial interests or personal relationships that could have appeared to influence the work reported in this paper.

#### Acknowledgments

This work was supported by Science and Technology Major Project of Inner Mongolia Autonomous Region in China (No. 2021ZD0028), the National Natural Science Foundation of China (Grant Number 51975343), Shanghai Qingpu District Industry-University-Research

Cooperation Development Fund (No. 2022-7), and Shanghai Technical Service Center for Advanced Ceramics Structure Design and Precision Manufacturing (No. 20DZ2294000).

#### References

- [1] Y. Dong, H. Lei, W. Liu, Effect of mixed-shaped silica sol abrasives on surface roughness and material removal rate of zirconia ceramic cover, *Ceram. Int.* 46 (2020) 23828–23833, <https://doi.org/10.1016/J.CERAMINT.2020.06.159>.
- [2] K. Kim, D.K. Yi, U. Paik, Increase in Ce<sup>3+</sup> concentration of ceria nanoparticles for high removal rate of SiO<sub>2</sub> in chemical mechanical planarization, *ECS J. Solid State Sci. Technol.* 6 (2017) 681–685, <https://doi.org/10.1149/2.0371709jss>.
- [3] L. Zhang, S. Raghavan, M. Weling, Minimization of chemical-mechanical planarization (CMP) defects and post-CMP cleaning, *J. Vac. Sci. Technol. B: Microelectron. Nanom. Struct. Process. Meas. Phenom.* 17 (1999) 2248, <https://doi.org/10.1116/1.590901>.
- [4] Z. Zhang, L. Yu, W. Liu, Z. Song, Surface modification of ceria nanoparticles and their chemical mechanical polishing behavior on glass substrate, *Appl. Surf. Sci.* 256 (2010) 3856–3861, <https://doi.org/10.1016/J.APSUSC.2010.01.040>.
- [5] J. Cheng, S. Huang, Y. Li, T. Wang, L. Xie, X. Lu, RE (La, Nd and Yb) doped CeO<sub>2</sub> abrasive particles for chemical mechanical polishing of dielectric materials: experimental and computational analysis, *Appl. Surf. Sci.* 506 (2020), 144668, <https://doi.org/10.1016/J.APSUSC.2019.144668>.
- [6] C. Zhou, X. Xu, L. Dai, H. Gong, S. Lin, Chemical-mechanical polishing performance of core-shell structured polystyrene@ceria/nanodiamond ternary abrasives on sapphire wafer, *Ceram. Int.* 47 (2021) 31691–31701, <https://doi.org/10.1016/J.CERAMINT.2021.08.048>.
- [7] Z. Zhang, Z. Shi, Y. Du, Z. Yu, L. Guo, D. Guo, A novel approach of chemical mechanical polishing for a titanium alloy using an environment-friendly slurry, *Appl. Surf. Sci.* 427 (2018) 409–415, <https://doi.org/10.1016/J.APSUSC.2017.08.064>.
- [8] Z. Zhang, L. Liao, X. Wang, W. Xie, D. Guo, Development of a novel chemical mechanical polishing slurry and its polishing mechanisms on a nickel alloy, *Appl. Surf. Sci.* 506 (2020), 144670, <https://doi.org/10.1016/J.APSUSC.2019.144670>.
- [9] Z. Zhang, J. Cui, J. Zhang, D. Liu, Z. Yu, D. Guo, Environment friendly chemical mechanical polishing of copper, *Appl. Surf. Sci.* (2019) 467–468, <https://doi.org/10.1016/J.APSUSC.2018.10.133>, 5–11.
- [10] L. Liao, Z. Zhang, F. Meng, D. Liu, J. Liu, Y. Li, X. Cui, Novel rotary chemical mechanical polishing on an integral impeller, *J. Manuf. Process.* 66 (2021) 198–210, <https://doi.org/10.1016/J.JMAPRO.2021.04.010>.
- [11] W. Xie, Z. Zhang, L. Liao, J. Liu, H. Su, S. Wang, D. Guo, Green chemical mechanical polishing of sapphire wafers using a novel slurry, *Nanoscale* 12 (2020) 22518–22526, <https://doi.org/10.1039/DONR04705H>.
- [12] K.S. Park, Z. Ni, A.P. Côté, J.Y. Choi, R. Huang, F.J. Uribe-Romo, H.K. Chae, M. O’Keeffe, O.M. Yaghi, Exceptional chemical and thermal stability of zeolitic imidazolate frameworks, *Proc. Natl. Acad. Sci. U.S.A.* 103 (2006) 10186–10191, <https://doi.org/10.1073/PNAS.0602439103>.
- [13] Y. Chen, X. Li, M.U. Nisa, J. Lv, Z. Li, ZIF-67 as precursor to prepare high loading and dispersion catalysts for Fischer-Tropsch synthesis: particle size effect, *Fuel* 241 (2019) 802–812, <https://doi.org/10.1016/J.FUEL.2018.12.085>.
- [14] J. Cui, T. Liu, Q. Zhang, T. Wang, X. Hou, Rapid microwave synthesis of Fe<sub>3</sub>O<sub>4</sub>-PVP/ZIF-67 as highly effective peroxyoxonolysulfate catalyst for degradation of bisphenol F and its mechanism analysis, *Chem. Eng. J.* 404 (2021), 126453, <https://doi.org/10.1016/J.CEJ.2020.126453>.
- [15] Q. Li, S. Jiang, S. Ji, M. Ammar, Q. Zhang, J. Yan, Synthesis of magnetically recyclable ZIF-8@SiO<sub>2</sub>/Fe<sub>3</sub>O<sub>4</sub> catalysts and their catalytic performance for Knoevenagel reaction, *J. Solid State Chem.* 223 (2015) 65–72, <https://doi.org/10.1016/J.JSSC.2014.06.017>.
- [16] Y. Pan, Y. Liu, G. Zeng, L. Zhao, Z. Lai, Rapid synthesis of zeolitic imidazolate framework-8 (ZIF-8) nanocrystals in an aqueous system, *Chem. Commun.* 47 (2011) 2071–2073, <https://doi.org/10.1039/C0CC05002D>.
- [17] C. Ramesh Kumar, M. Omkumar, Optimisation of process parameters of chemical mechanical polishing of soda lime glass, *Silicon* 11 (2018) 407–414, <https://doi.org/10.1007/S12633-018-9903-3>.
- [18] C. Ho, J.C. Yu, T. Kwong, A.C. Mak, S. Lai, Morphology-controllable synthesis of mesoporous CeO<sub>2</sub> nano- and microstructures, *Chem. Mater.* 17 (2005) 4514–4522, <https://doi.org/10.1021/cm0507967>.
- [19] A. Iqbal, A.S. Ahmed, N. Ahmad, A. Shafi, T. Ahamad, M.Z. Khan, S. Srivastava, Biogenic synthesis of CeO<sub>2</sub> nanoparticles and its potential application as an efficient photocatalyst for the degradation of toxic amido black dye, *Environ. Nanotechnol. Monit. Manag.* 16 (2021), 100505, <https://doi.org/10.1016/J.ENNM.2021.100505>.
- [20] Y. Chen, Z. Li, N. Miao, Polymethylmethacrylate (PMMA)/CeO<sub>2</sub> hybrid particles for enhanced chemical mechanical polishing performance, *Tribol. Int.* 82 (2015) 211–217, <https://doi.org/10.1016/j.triboint.2014.10.013>.
- [21] K.S.W. Sing, D.H. Everett, R.A.W. Haul, L. Moscou, R.A. Pierotti, J. Rouquerol, T. Siemieniewska, Reporting physisorption data for gas/solid systems with special reference to the determination of surface area and porosity, *Pure Appl. Chem.* 57 (1985) 603–619, <https://doi.org/10.1351/pac198557040603>.
- [22] Y. Chen, R. Long, Polishing behavior of PS/CeO<sub>2</sub> hybrid microspheres with controlled shell thickness on silicon dioxide CMP, *Appl. Surf. Sci.* 257 (2011) 8679–8685, <https://doi.org/10.1016/J.APSUSC.2011.05.047>.
- [23] L.M. Cook, Chemical processes in glass polishing, *J. Non-Cryst. Solids* 120 (1990) 152–171, [https://doi.org/10.1016/0022-3093\(90\)90200-6](https://doi.org/10.1016/0022-3093(90)90200-6).

- [24] T. Hoshino, Y. Kurata, Y. Terasaki, K. Susa, Mechanism of polishing of SiO<sub>2</sub> films by CeO<sub>2</sub> particles, *J. Non-Cryst. Solids* 283 (2001) 129–136, [https://doi.org/10.1016/S0022-3093\(01\)00364-7](https://doi.org/10.1016/S0022-3093(01)00364-7).
- [25] R. Srinivasan, P.V. Dandu, S.V. Badu, Shallow trench isolation chemical mechanical planarization : a review, *ECS J. Solid State Sci. Technol.* 4 (2015) 5029–5039, <https://doi.org/10.1149/2.0071511jss>.
- [26] Z. Hong, X. Niu, Y. Liu, C. Yang, Y. Lu, Application and mechanism of complexing agent DTPA-5K in barrier CMP of integrated circuit, *Electron. Components Mater.* 40 (2021) 156–162, <https://doi.org/10.14106/j.cnki.1001-2028.2021.1771>.
- [27] Y.G. Wang, L.C. Zhang, A. Biddut, Chemical effect on the material removal rate in the CMP of silicon wafers, *Wear* 270 (2011) 312–316, <https://doi.org/10.1016/J.WEAR.2010.11.006>.
- [28] R. Ding, H. Lei, L. Xu, Y. Chen, Surface planarization of zirconia ceramic achieved by polyacrylamide grafted nanodiamond composite abrasives through chemical mechanical polishing, *Ceram. Int.* 48 (2022) 19900–19912, <https://doi.org/10.1016/j.ceramint.2022.03.265>.
- [29] A. Pfau, K.D. Schierbaum, The electronic structure of stoichiometric and reduced CeO<sub>2</sub> surfaces: an XPS, UPS and HREELS study, *Surf. Sci.* 321 (1994) 71–80, [https://doi.org/10.1016/0039-6028\(94\)90027-2](https://doi.org/10.1016/0039-6028(94)90027-2).
- [30] B. Ge, T. Yue, J. Liu, Use and mis-use of x-ray photoemission spectroscopy Ce3d spectra of Ce<sub>2</sub>O<sub>3</sub> and CeO<sub>2</sub>, *J. Phys. Condens. Matter* 30 (2018), 343003, <https://doi.org/10.1088/1361-648X/AAD248>.
- [31] J. Zhang, H. Wong, D. Yu, K. Kakushima, H. Iwai, X-ray photoelectron spectroscopy study of high-k CeO<sub>2</sub>/La<sub>2</sub>O<sub>3</sub> stacked dielectrics, *AIP Adv.* 4 (2014), 117117, <https://doi.org/10.1063/1.4902017>.
- [32] K. Storck, D. Loyd, B. Augustsson, Heat transfer modelling of the parison forming in glass manufacturing, *Glass Technol.* 39 (1998) 210–216 (accessed 20 April 2022), <https://www.ingentaconnect.com/content/sgt/gt/1998/00000039/00000006/3906210>.
- [33] R. Sabia, H.J. Stevens, Performance characterization of cerium oxide abrasives for chemical-mechanical polishing of glass, *Mach. Sci. Technol.* 4 (2000) 235–251, <https://doi.org/10.1080/10940340008945708>.
- [34] E. Kim, J. Hong, S. Hong, C. Kanade, H. Seok, H.U. Kim, T. Kim, Improvement of oxide removal rate in chemical mechanical polishing by forming oxygen vacancy in ceria abrasives via ultraviolet irradiation, *Mater. Chem. Phys.* 273 (2021), 124967, <https://doi.org/10.1016/J.MATCHEMPHYS.2021.124967>.
- [35] T. Sugimoto, S. Suda, K. Kawahara, Change in slurry/glass interfacial resistance by chemical mechanical polishing, *MRS Adv.* 2 (2017) 2205–2210, <https://doi.org/10.1557/ADV.2017.335>.
- [36] N. Ozawa, M. Ishikawa, M. Nakamura, M. Kubo, Polishing process simulation of SiO<sub>2</sub> by CeO<sub>2</sub> abrasive grain under wet environment, *Hyomen Kagaku* 33 (2012) 351–356, <https://doi.org/10.1380/JSSSJ.33.351>.